IEEE Access
Multidisciplinary ⋮ Rapid Review ⋮ Open Access Journal

Received December 24, 2019, accepted January 17, 2020, date of publication January 28, 2020, date of current version February 11, 2020.

Digital Object Identifier 10.1109/ACCESS.2020.2970115

Coordinated Intersection Signal Design for Mixed Traffic Flow of Human-Driven and Connected and Autonomous Vehicles

HONGSHENG QI[1], RUMENG DAI[1], QING TANG[2], AND XIANBIAO HU[2]
[1]Department of Civil Engineering, Zhejiang University, College of Civil Engineering and Architecture, Hangzhou 310058, China
[2]Department of Civil, Architectural and Environmental Engineering, Missouri University of Science and Technology, Rolla, MO 65409, USA

Corresponding author: Xianbiao Hu (xbhu@mst.edu)

This work was supported in part by the Key Research and Development Program of China under Grant 2018YFB1600900, in part by the Key Research and Development Program of Zhejiang under Grant 2018C01007, and in part by the Zhejiang Province Public Welfare Scientific Research Project under Grant LGF18E080003.

ABSTRACT This manuscript investigated coordinated intersection signal design problem for mixed traffic flow of Human-Driven Vehicles (HDVs) and Connected and Autonomous Vehicles (CAVs). Two main macroscopic impact of the mixed flow on signal setting are considered: saturation flow rate and the platoon dispersion. In order to capture the traffic flow operational characteristics on coordinated intersections, three locations, namely entrance location where the loop detector was located at, and upstream intersection and downstream intersection were defined. Two types of vehicle cumulative curves, namely cumulative arrival profile and cumulative departure profile were constructed. The mixed-flow traffic dynamics were analyzed, and the arrival-departure curves relationship was derived using a combination of Newell car-following and Akçelik acceleration model. A mixed-flow platoon dispersion model was proposed to describe the vehicle's progression between two locations. Due to the nonlinear nature of the problem, a particle swarm optimization (PSO) method was employed to obtain the optimal signal parameters, including the cycle length, green duration, and optimal offset. The algorithm was implemented and validated in a case study involving two intersections, with the demand formulated and simulated by the Markov chain. The results showed that the proposed model could effectively decrease delays when compared with current signal control methods.

INDEX TERMS Coordinated signal control, connected and autonomous vehicles, cumulative curves, platoon dispersion, traffic flow modeling.

I. INTRODUCTION

Connected and autonomous vehicle (CAV) technologies endow great potentials for future transportation systems. CAV technologies can be decomposed into connected vehicles (CV) and autonomous vehicles (AV). With the former technology, vehicles can communicate with each other (known as V2V) and infrastructure (known as V2I) or even communicate with pedestrians (known as V2P). Together, they are named V2X. With respect to the latter one, according to the U.S. Department of Transportation [16], the autonomous level can be classified into six levels, from level zero (L0) to level five (L5). AVs can detect traffic flow dynamics, such as real time distance between the host vehicle and other vehicles, the speed of other vehicles and the pedestrians, etc. with on-board sensors that include a camera, Lidar, and so on. Compared with human driven vehicles (HDV), CAVs have many advantages but, of most importance, CAVs behave accurately, as they are controlled by the algorithms, and there is no reaction delay in the high computation power of today's processors.

Current traffic control systems work using the following procedures: (1) First, the demand, or arrival flow rate, is determined. This can be detected by loop detectors or other sensors, including a camera, magnetic detectors, etc. (2) Given traffic demand, a variety of Performance Indexes (PI) can be computed, such as delay, stops, etc. These PIs are calculated given the saturation flow rate, which is assumed fixed and independent on the arrival demand. (3) A signal plan is chosen that best corresponds to the PI (such as traffic delay and number of stops), and the system implements these signal parameters. Typical parameters include cycle length, green split, offset.

With the advancement of CAV technologies, the traffic control systems that were designed for only HDVs are currently facing new challenges. One of the fundamental reasons

The associate editor coordinating the review of this manuscript and approving it for publication was Bohui Wang.

is that CAVs can react to traffic flow changes in a way that is not only much faster but also more accurate than HDVs. Therefore, many of the microscopic traffic flow dynamics are different, indicating if the same signal planning method is to be used, the results would be unsatisfactory. Take the platoon dispersion behavior of the discharging vehicles, which is a key factor that influences traffic signal coordination as an example. The reason that platoon dispersion occurs is that different vehicles operate in various speeds and, hence, the same upstream departure eventually leads to different downstream arrivals. As CAVs behave accurately, and their speed variances becomes minimal, or even zero, the signal coordination scheme which is currently designed for only the HDVs platoon may not perform well for mixed traffic flows that include both HDVs and CAVs.

Signal control for a CAV environment has received significant research attention. For instance, Beak *et al.* [2] used connected vehicle trajectory to optimize the coordinated signal settings. The algorithm worked at two levels–one at intersection level and the other at corridor level. Dresener and Stone [6] developed an Autonomous Intersection Management (AIM) protocol which was free of traffic signals. The vehicles called ahead to reserve a time interval and, then, the intersection decided whether to assign an interval or not. Such a model was extended to multi intersections by Hausknecht *et al.* [8]. In this extended coordination algorithm, the navigation policy of CAV was combined. Lee *et al.* [12] studied the sustainable control of multi-intersections for CVs, which obeyed the commands of controllers. This type of control was also named ''signal-free'' control. However, the problem of intersection coordination control for the mixed traffic flows of HDVs and CAVs had not yet been well investigated. Another type of research is to optimize the signal and the CAV trajectories simultaneously. The objectives of the cooperative control include efficiency, eco and safety. For instance, Yu *et al.* [26] optimized the trajectories and the signal at single intersection simultaneously. The CAV vehicles passed the intersection in a platoon style; Xu *et al.* [24] also proposed a cooperative control method of signal and vehicles trajectories. The fuel consumption was taken into account; Guo *et al.* [5] studied the joint optimization of signal and the trajectories at the same time. The numerical scenario was common four-phase but can be extended to other cases.

This manuscript investigated coordinated intersection signal design problem for mixed traffic flows of Human-Driven Vehicles and Connected and Autonomous Vehicles. In order to capture the two main influences of mixed flow, namely the saturation flow rate (SFR) and the platoon dispersion, three locations, namely entrance location where the loop detector was located at, and upstream intersection and downstream intersection were defined. Two types of vehicle cumulative curves, namely cumulative arrival profile and cumulative departure profile were constructed. The mixed-flow traffic dynamics were analyzed, and the arrival-departure curves relationship was derived using a combination of Newell car-following and Akçelik acceleration model. A mixed-flow platoon dispersion model was proposed to describe the vehicle's progression between two locations. Due to the nonlinear nature of the problem, a particle swarm optimization (PSO) method was employed to obtain the optimal signal parameters, including the cycle length, green duration, and optimal offset. This research mainly considers the signal optimization given arrival mixed demand. Although the control of CAV using SPaT information is possible [26], it can be foreseen that in the near future, most intersections are operated without the proactive control of CAVs. Thus it is important to understand the impact of mixed flow on the traffic flow operational characteristics: the saturation flow rate at the stop line and the platoon dispersion behavior [28]. The above two influences brought by mixed flow and the resulting signal optimization performances are the main focus of our study, although there are many other influences [27]. Also note that, the signal settings are implemented for movements, rather than single vehicle. There exist a variety of headway preferences of drivers. Extend of the proposed model to accommodate the headway variety is easy.

The structure of this paper was organized as follows. The model formulation for mixed-flow coordinated intersection signal control was presented in Section 2. The model took in the mixed flows arrival information at entrance location as the input data, and outputted the departure profile, as well as delays and stops at the downstream intersection location. The proposed model was implemented and tested in Section 3, and Section 4 provided a conclusion for this approach, along with a discussion of future work.

II. MODEL FORMULATION

A. NOTATIONS

As a convenient reference, the mathematical notations used in this section are presented below.

HDV and CAV: human driven vehicles and connected and autonomous vehicles;
$N_{i,W,TH}(t)$, $D_{i,W,TH}(t)$, $Q_{i,W,TH}(t)$: arrival, departure cumulative vehicle count and queued vehicle count at intersection i for west approach, through movement;
$N^{-1}_{i,W,TH}(j)$: the moment when the cumulative arrival vehicle count is j at intersection i;
$D^{-1}_{i,W,TH}(j)$ the moment when the cumulative departure vehicle count is j at intersection i;
$d_{i,i+1}$: distance between intersection i and $i+1$;
v_{min} and v_{max}: the minimal and maximal speed for truncated normal distribution;
$\tilde{v}$: speed limit
m: parameter in the Akcelik acceleration profile model;
t_a: time for acceleration used in Akcelik acceleration profile model;
a_{max}: maximum acceleration in the Akcelik acceleration profile model; d_{jam}: the distance between the front bumper of the leading vehicle and following vehicle when the speed is zero.

τ_{HDV} and τ_{CAV}: the reaction delay of human driven vehicles and connected and autonomous vehicles.
h_{CAV}, h_{HDV}: the stable headway for CAVs and HDVs.
$f_V(v)$: the speed distribution of HDVs
g_e: the green duration required for the queue to be completely cleared.
g_{min} and g_{max}: the minimal and maximal green duration;
C_{min} and C_{max}: the minimal and maximal cycle length;
t_{yellow}: yellow time;
S: saturation flow rate.
t_{loss}: startup loss time and stop loss time;
$PI_{D,i}$: the total delay of intersection i;
$PI_{S,i}$: the number of stops of intersection i;
$\mathcal{A}, \mathcal{D}$: used to indicate the approach and turning directions. $\mathcal{A} \in \{E, W, S, N\}$ which means east, west, south and north; $\mathcal{D} \in \{L, TH, R\}$, which means left, through and right;
$\mathcal{K}$(t): the arrival cycle index for moment t;
ξ: the interval between neighboring arrival types;
$f_\xi(t)$ is the distribution of interval ξ;
$\pi = [\pi_{HDV}, \pi_{CAV1}, \pi_{CAV2}]$: the probability of each arrival type including HDV, CAV1 and CAV2. The last type is the batch arrival with smaller headway;
Π_1, Π_3 and Π_3: three π settings in the experiment. They are [0.1, 0.1, 0.8], [0.1, 0.8, 0.1] and [0.8, 0.1, 0.1] respectively.
ϕ: the mean arrival vehicles count for CAV2;
$\mathbb{S}_j$: the 'velocity' of the j_{th} particle during the PSO optimization; $\mathbb{S}_{max}$ is the maximal allowed velocity;

B. DEPARTURE-ARRIVAL PROFILE MODELING FRAMEWORK

This subsection presents the modeling framework of this manuscript based on the key concept of cumulative departure profile curve and cumulative arrival profile curve. As shown in FIGURE 1, The study area in the figure consists three locations, namely entrance location where the loop detector is located at, upstream intersection, and downstream intersection. It should be noted although only two intersections are shown in this figure, the developed model can be applied iteratively for a network with more intersections. It is assumed that each intersection is equipped with a road side unit (RSU), with a detection range of about 500 m to 1000 m (Dey *et al.*, [3]). This allows the system to obtain arrival information for vehicles. It is assumed that the vehicle type is also known (HDV or CAV) to the intersections systems and, therefore, the arrival demand could be represented by using a flow rate curve or a cumulative curve.

Upon obtaining the arrival vehicles information at the entrance location, the system captures the traffic flow dynamics in four steps, as indicated in FIGURE 1. Suppose that an arrival at the entrance location is indicated by cumulative profile $N_{i,W,CAV}(t)$ and $N_{i,W,HDV}(t)$, the model works as follows:

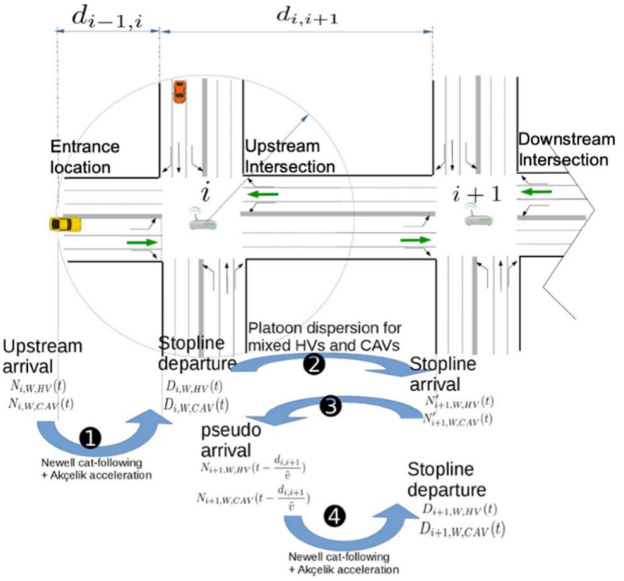

FIGURE 1. Study area description and model framework.

1) Uses Newell car following model and Akçelik acceleration model to get the departure profile at upstream intersection i, $D_{i,W,HDV}(t)$ and $D_{i,W,CAV}(t)$.
2) Uses platoon dispersion model to capture the expected arrival profile at downstream intersection i+1, $N'_{i+1,W,CAV}(t)$ and $N'_{i+1,W,HDV}(t)$.
3) As the expected arrival at downstream intersection is measured at the stop-line location, we need to translate this expected arrival to a pseudo arrival profile at the upstream location, $N_{i+1,W,CAV}(t)$ and $N_{i+1,W,HDV}(t)$.
4) Again, the Newell car-following and Akçelik acceleration model can be employed to obtain the departure profile at downstream intersection i+1.

In step 1, the vehicles are treated as exogenous flow and, therefore, the microscopic traffic flow behavior is different from the flow traverse from intersection i to i+1 in step 2, which experiences a platoon dispersion. For the model component of step 3, as the Newell car following model cannot capture the dispersion effect of platoons of mixed flow, the dispersed cumulative arrival $N'_{i+1,HDV}(t)$ needs to be projected to the road entrance of this intersection, i.e. $N_{i+1,HDV}(t) = N'_{i+1,HDV}(t+d_{i,i+1}/\tilde{v})$. Then, in step 4 we can use the same method as step 1 to describe the departure profile at downstream intersection i+1.

The next several subsections are devoted to the presentation of mixed-flow traffic dynamic analysis and the methodologies for step 1 and step 2. The detailed presentation of step 3 is skipped as it's mostly an horizontal shift of the cumulative curve, and discussion on step 4 is not repeated either as the key methodology is the same as step 2.

C. MIXED-FLOW TRAFFIC DYNAMICS ANALYSIS

Prior to the presentation of the four-step model, this section analyzes the traffic dynamics of mixed flow of HDVs and

CAVs, which reveals the intrinsic microscopic traffic flow behavior and will be referred back often in future sections later on. The resulting startup loss time and saturation flow rate, which are two key inputs to the traffic signal design, will also be analyzed.

It has been generally recognized that, after the onset of a green signal, most HDVs pass the stop line with a decreasing headway. The first several headways are relatively high, due to the fact that these vehicles have not accelerated enough. After the 4th or 5th vehicle passes the stop-line, the following headways remain relatively stable and are lower. The inverse of a stable headway is defined as ''saturation flow rate'' and the underlying headway is defined as ''saturated headway''. According to field observation, a saturated headway was about 2s (this value was observed for an environment that had only HDVs).

CAVs, on the other hand, can timely and accurately react to changes in the status of the leading vehicles, and, hence, behave differently than HDVs. To investigate the headway behavior of a mixed CAV flow, we resort to the Newell simplified car following model (Ni [17]) which works as shown in FIGURE 2. There are two vehicles - one is the lead vehicle and one follower vehicle. The two vehicles are expressed as bold lines. Before time t, both vehicles travel at speed v_1. At time t, the leading vehicle slows down to speed v_2 and, after a time duration τ, the following vehicle also changes its speed to v_2. The spacing before moment t and after moment $t+\tau$ is s_1 and s_2, respectively. The headway at location x_1 is h_1 and at location x_2 is h_2. The above description implies that, when using the Newell car following model, one just needs to move the leading vehicle's trajectory horizontally (i.e., spatially) by d_{jam} and vertically (i.e., temporally) by τ, so that the resulting trajectory becomes the following vehicle's trajectory. The parameters τ and d_{jam} are independent of the speed. τ could be interpreted as the perception reaction time, and d could be interpreted as the jam density. We could derive that $h_1 = \tau + d_{jam}/v_1$ and $h_2 = \tau + d_{jam}/v_2$. If the speed limit is $\tilde{v}$, the stable headway could be derived by $\tau + d_{jam}/\tilde{v}$. When the jam density is given, the jam distance between two vehicles, i.e. d_{jam} is also fixed. As the jam density is relatively fixed, the headway depends on parameters τ and speed limit.

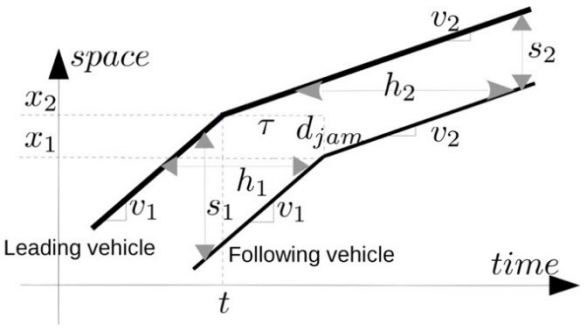

FIGURE 2. Newell simplified method.

The reaction time of human drivers consists of several parts (Gartner *et al.* [4]), including perception latency, eye movement, fixation, recognition, and initiation brake action. The total duration could reach 2.74 s. However,s this number varies for different drivers. We use the settings by Wei *et al.* [22], i.e., the perception time is 1.3 and the response delay is 0.4 s. Thus, the total delayed reaction is 1.7 sec. For CAV, the delay consists of a communication delay, and computer processing time. Compared with HDVs, the reaction delay could be reduced drastically. We symbolize the reaction delay of HDV as τ_{HDV} and the reaction delay of CAV as τ_{CAV}. Given the trajectory of the leading vehicle, the parameters τ and d_{jam} would determine the trajectory of the following vehicle and, in-turn, determine the headways.

The vehicles accelerate when the green starts. According to Akçelik and Besley [1], the acceleration from zero speed to the terminal speed (usually the speed limit) is not constant and could be described by the following formula:

$$a(t) = \frac{(1+2m)^{2+\frac{1}{m}}}{4m^2} a_{max} \frac{t}{t_a} \left(1 - \left(\frac{t}{t_a}\right)^{m}\right)^{2} \tag{1}$$

In Eq. (1), t is the moment from the beginning of acceleration, m is a parameter, a_{max} is the maximum acceleration, and t_a is the acceleration duration. The resulting velocity profile and trajectory profile are given by the following equations:

$$v(t) = v_{init} + \frac{3.6\,(1+2m)^{2+\frac{1}{m}}}{4m^2} a_{max} t_a \left(\frac{t}{t_a}\right)^{2} \times \left[0.5 - 2\frac{\left(\frac{t}{t_a}\right)^{m}}{m+2} + \frac{\left(\frac{t}{t_a}\right)^{2m}}{2m+2}\right] \tag{2}$$

$$x(t) = v_{init}\frac{t}{3.6} + \frac{(1+2m)^{2+\frac{1}{m}}}{4m^2} a_{max} t_a^2 \left(\frac{t}{t_a}\right)^{3} \times \left[\frac{1}{6} - 2\frac{\left(\frac{t}{t_a}\right)^{m}}{(m+2)\,(m+3)} + \frac{\left(\frac{t}{t_a}\right)^{2m}}{(2m+2)(2m+3)}\right] \tag{3}$$

v_{init} in Eq. (2) is the initial speed. When the vehicle begins to accelerate, the initial speed is 0. The acceleration profile given by Eq. (1) satisfies many requirements, such as zero acceleration and jerk at the start and end of the process. Using the result of $m = 0.587$ in Akçelik and Besley [1], FIGURE 3, FIGURE 4, and FIGURE 5 give the distance profile (measured from the stop-line), acceleration profile, and speed profile for the speed limits of 50km/h and 70km/h. The maximum acceleration is $2.8 m/s^2$ and $2.9 m/s^2$, respectively. It can be observed in FIGURE 3 that the moment when the first vehicle passes the stop-line depends on the context parameters. When the starting wave propagates to upstream, the vehicles in the queue pass the intersection, consecutively, and the headways gradually change.

To investigate the evolution of the headway and uncover its influence on the mixed HDVs and CAV flows, we use the

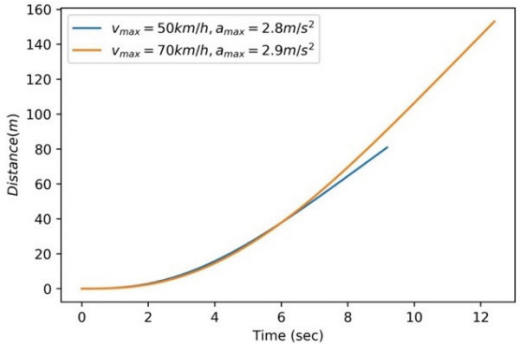

FIGURE 3. Distance profiles using model in Akçelik and Besley (2001).

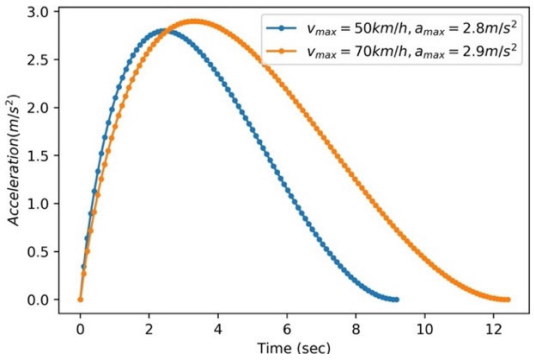

FIGURE 4. Acceleration profiles using model in Akçelik and Besley (2001).

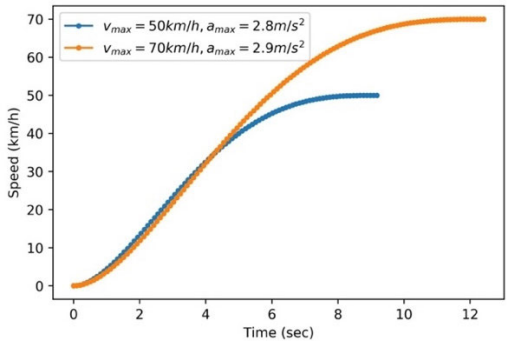

FIGURE 5. Speed profiles using model in Akçelik and Besley (2001).

Newell simplified car following model to construct the trajectories of the vehicles. These procedures are shown in FIGURE 6. The first vehicle (ID=0) enters the road at moment t_0. The road speed limit is $\tilde{v}$. The expected arrival moment at the stop-line is t'_0, which is within the green domain and, hence, the vehicle with ID=0 could pass the intersection. The following vehicle is with ID=1, and enters the road at moment t_1. Its expected arrival time at the stop-line is t'_1, which encounters a red duration. This expected trajectory does not intersect with the spatial-temporal translated trajectory of the vehicle with ID=0. Therefore, the vehicle with ID=1 is not influenced by its leading vehicle, but it is influenced by the red signal. The deceleration profile (including the distance profile, deceleration rate and speed profile) could also be derived by Eq. (2) and Eq. (3), using speed limit as the initial speed and negative acceleration. When the speed limit and the maximum deceleration are given, the deceleration distance is

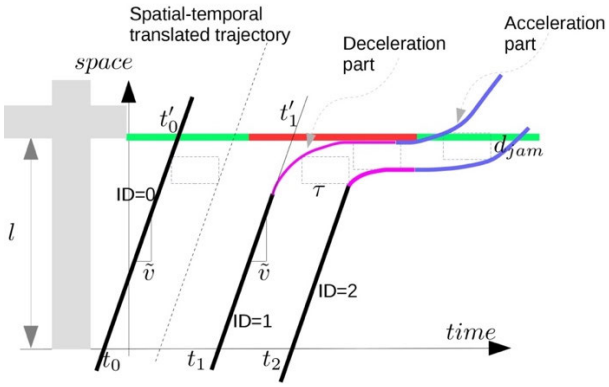

FIGURE 6. Newell car following for acceleration and deceleration.

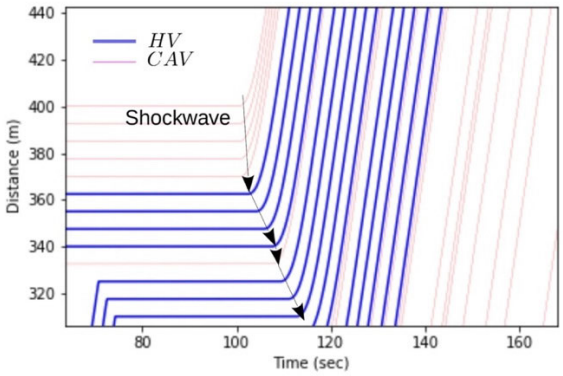

FIGURE 7. One snapshot of the trajectories.

also known and, therefore, the trajectory of the vehicle with ID=1 could be obtained by combing the deceleration distance profile and the upstream free-flow trajectory. After the vehicle stopped, the speed reaches 0. After the onset of green, the vehicle with ID=1 accelerates with a known profile given by Eq. (2) and Eq. (3). The trajectory of vehicle ID=1 is then obtained. The vehicle with ID=2 intersects with the spatial-temporal translated trajectory of vehicle ID=1 and, therefore we join the free-flow trajectory before the intersection point and the translated trajectory after the intersection point, allowing the trajectory of the vehicle with ID=2 to be derived. In this way, each trajectory could be solved one by one.

It should be noted that, when constructing a deceleration profile, the speed may change instantly, rather than gradually. This is caused by a shortcoming of the Newell car following model when describing non-equilibrium behavior. However, as we are concerned with the headways, the deceleration profiles do not influence the moments when a vehicle passes the stop-line. Also, note that, in FIGURE 6, with different parameters, such as τ_{HDV} and τ_{CAV}, we have different trajectories representing various vehicle properties. The resulting headways also reflect different vehicle types.

We use the setting of $\tau_{HDV} = 1.7$ and $\tau_{CAV} = 0.1$ to simulate the departure trajectories; the results are given in FIGURE 7. The stop-line is located at the spatial coordinate of 400m. The speed limit is 50km/h. Bold lines are HDVs

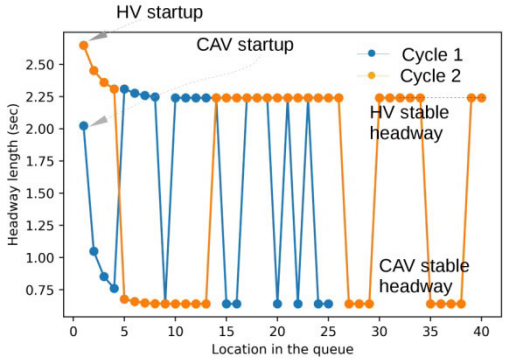

FIGURE 8. Headways series for two cycles.

and thin lines are CAVs. Compared with HDVs, the CAVs follow more closely. The shockwave generated by the two types of vehicles are also given, and it shows that the wave of CAVs propagates faster than that of HDVs. In FIGURE 7, the first five vehicles are CAV, while there are four HDV followers. The headways generated by such mixed arrival flows are given in FIGURE 8, which contains the headways series of two cycles. A headway is defined as the "time difference between the moments when two neighboring vehicles pass the stop-line". Note that these vehicles must accelerate from 0 speed, i.e. these vehicles must experience a full stop, otherwise the headways are influenced, not only by the signal but also by the arrival law. The moment when a vehicle passes the stop-line can be interpolated from the spatial-temporal trajectory. These trajectories are generated by the above acceleration model and the Newell car-following model. Therefore, we have the headways series. The first cycle data in FIGURE 8 coincides with that of the platoons in FIGURE 7.

In FIGURE 8, we can observe that the first cycle headways series begin from about 2 sec and decrease drastically to 1.00 sec. For the second cycle, the headways series begin from about 2.6 sec and, then, also decrease to about 2.4 sec. It can be easily inferred that the first four vehicles in the queue in cycle 2 are HDVs. Hence, the CAVs and HDVs generate different headways characteristics, even though the acceleration profiles are the same. It can also be observed that there are two possible headways when the vehicles are accelerated enough. The higher one is 2.25 sec while the lower one is about 0.6sec. It is easy to tell that the former one is HDV and the latter one is CAV. Actually, stable headways can be calculated from $\tau + \mathrm{d_{jam}}/\tilde{v}$. Using $\tau_{\mathrm{HDV}} = 1.7$, $\tilde{v} = 50\mathrm{km/h}$ and $\mathrm{d_{jam}} = 7.5m$, we have a stable headway at 2.24sec. Using $\tau_{\mathrm{HDV}} = 0.1$, we have a stable headway at 0.64 sec.

Next, we investigate the startup loss time, which is defined and calculated using the method shown in FIGURE 9. Differences between the headways and the stable headways are indicated by using $\delta \mathrm{t}_1, \delta \mathrm{t}_2, \ldots$ etc., after reaching a certain number, $\delta \mathrm{t_n} = 0$. The startup loss is defined as $\sum_{i=1}^{n} \delta \mathrm{t_i}$. The headways depend on the speed limit $\tilde{v}$ and maximum acceleration $\mathrm{a_{max}}$. FIGURE 10 shows the startup loss time when $\mathrm{a_{max}} = 2.9m/s^2$. The startup loss time increases linearly with the speed limit, due to the fact that the acceleration duration also increases when the maximum acceleration is fixed. However, this conclusion should not be generalized since acceleration profiles may differ from vehicle to vehicle. Also, it can be concluded that the startup loss times are the same for pure HDVs flow and pure CAVs flow at signalized intersections, as the curves for pure HDV and CAV overlap accurately.

FIGURE 11 gives the headways distributions when flows are mixed - half HDVs and half CAVs. The red and green durations are both 100 sec, and we simulated 30 cycles and collected the headways. It can be seen that the headways have two clusters: one around 2.24 sec and one around 0.64 sec. The former one is for HDVs and the latter one for CAVs.

Next, we compute the intersection capacity when the flow is mixed HDVs and CAVs, under fixed signal settings. Suppose the intersection is a common four-leg intersection and that four phases are: north-bound (NB) through and south-bound (SB) through, NB & SB left, WB & EB through, and WB & EB left (for simplicity we neglect the right-turn movements). Suppose that, after a certain number n, startup loss diminishes to zero, i.e., $\delta_{\mathrm{n+1}} = 0$ and $\delta_{\mathrm{n}} > 0$. Suppose that the percentage of HDVs and CAVs are $\mathrm{p_{HDV}}$ and $\mathrm{p_{CAV}}$, respectively (we assume the percentage are uniform for all coming flows). The startup loss of location i for HDV and CAV are $\delta_{\mathrm{i,HDV}}$ and $\delta_{\mathrm{i,CAV}}$, respectively. Expectation of startup loss is calculated as:

$$\begin{aligned}
\mathrm{E}\left(\mathrm{t_{statup\ loss}}\right) &= \sum_{i=1}^{n}\left(\mathrm{p_{HDV}}\delta_{\mathrm{i,HDV}} + \mathrm{p_{CAV}}\delta_{\mathrm{i,CAV}}\right) \\
&= \sum_{i=1}^{n}\mathrm{p_{HDV}}\delta_{\mathrm{i,HDV}} + \sum_{i=1}^{n}\mathrm{p_{CAV}}\delta_{\mathrm{i,CAV}} \\
&= \mathrm{p_{HDV}}\sum_{i=1}^{n}\delta_{\mathrm{i,HDV}} + \mathrm{p_{CAV}}\sum_{i=1}^{n}\delta_{\mathrm{i,CAV}} \\
&= \left(\mathrm{p_{HDV}} + \mathrm{p_{CAV}}\right)\sum_{i=1}^{n}\delta_{\mathrm{i,CAV}} \\
&= \sum_{i=1}^{n}\delta_{\mathrm{i}} \qquad (4)
\end{aligned}$$

In the equation above, we use the constraint that $\mathrm{p_{HDV}} + \mathrm{p_{CAV}} = 1$. The expected headway is simply calculated as $\mathrm{p_{HDV}} * h_{HDV} + \mathrm{p_{CAV}} * h_{CAV}$. The capacity for the intersection could be calculated as (note that there are two lanes departing flow during green signals):

$$\begin{aligned}
\mathrm{CAP} &= 2 * \frac{C - 4 * \mathrm{E}\left(\mathrm{t_{statup\ loss}}\right)}{\mathrm{p_{HDV}}h_{HDV} + \mathrm{p_{CAV}}h_{CAV}} \\
&= 2 * \frac{C - 4\sum_{i=1}^{n}\delta_{\mathrm{i}}}{\mathrm{p_{HDV}}h_{HDV} + \mathrm{p_{CAV}}h_{CAV}} \qquad (5)
\end{aligned}$$

C in Eq. (5) is the cycle length. CAP depends on the cycle length and vehicles ratio. The results given by Eq. (5) includes 8 lanes. The capacity per lane could be obtained by dividing

the result by 8. It is plotted in FIGURE 12. With the same speed limit, a shorter headway brought by CAV could drastically lead to higher capacity at the signalized intersection. In all cases, the capacity at $p_{CAV} = 0.9$ is doubled when compared with $p_{CAV} = 0.1$. Many researchers proposed that, when the traffic flow is 100% CAV, a traffic signal is not necessary (Mirheli *et al.* [15]). This is an encouraging result, as a signal could work throughout a flow mixture range and, at the same time, the benefits are not inferior to the signal-free models.

D. DEPARTURE VEHICLE TRAJECTORY INTERPOLATION

This section presents the method to solve the first step problem, i.e. derive the departure profile at upstream intersection i, i.e. $D_{i,W,HDV}(t)$ and $D_{i,W,CAV}(t)$, with the loop detector data installed at the entrance location. At the entrance location or the location where the coordination begins (e.g., the western approach to intersection i in FIGURE 1), the vehicles arrive in sequence. Since the intersection could detect the arrival of vehicles, once a vehicle arrives (regardless if it is CAV or HDV), the intersection could predict the arrival of that vehicle at the stop-line using the Newell car following model and the Akçelik acceleration model. The arrival could be formulated as a cumulative vehicles curve $N_{i,W,TH}(t)$ for through-movement at the western approach to intersection i. Similarly, we have other approach demands: $N_{i,E,TH}(t)$, $N_{i,S,TH}(t)$, and $N_{i,N,TH}(t)$. We also get other turning directions demands: $N_{i,W,L}(t)$, $N_{i,W,R}(t)$ for left-turn and right-turn, respectively.

There are two cases for arrival: the vehicle could be either CAV or HDV. We split the demand $N_{i,W,TH}(t)$ into two sub-arrival cumulative vehicle numbers: $N_{i,W,TH,HDV}(t)$ and $N_{i,W,TH,CAV}(t)$. We have $N_{i,W,TH}(t) = N_{i,W,TH,HDV}(t) + N_{i,W,TH,CAV}(t)$, $\forall t$. Besides, some CAVs could operate in a platoon mode via corporative adaptive cruise control (CACC) technology. These CAVs are characterized by shorter headways, therefore, we further split the arrival of CAVs $N_{i,W,TH,CAV}(t)$ into two types: CAV type 1 $N_{i,W,TH,CAV1}(t)$ and CAV type 2 $N_{i,W,TH,CAV2}(t)$. CAVs arrival type 1 had only one vehicle, while type 2 is a batch arrival, which means that more than two vehicles are arriving together and the headways among these vehicles are identical. If there are neighboring two type 1 CAVs, the headway or distance between the two CAVs are different from the type 2. This is because the type 1 CAV operates under ACC mode while type 2 CAVs operate by CACC.

Once the intersection is aware of the arrival of the vehicles, the Newell car following, plus the Akçelik acceleration profile model could be used to track the trajectory of the vehicles and, hence, get the departure time from the stop-line. The departure times serve as the input to the next road sections. Without a loss of generality, we focus on the arrival-departure process of the western approach through movement at intersection i in FIGURE 1. Arrival at the upstream road entrance is $N_{i,W,TH}(t)$, while departure is $D_{i,W,TH}(t)$. We extend the method displayed in FIGURE 6 to several red signals, which are shown in FIGURE 13. The vehicle with ID=3 enters the road at moment t_3, i.e., point A. The figure also gives the spatial-temporal shifted trajectory of the vehicle with ID=2. The expected trajectory of the vehicle with ID=3 intersects with the spatial-temporal shifted trajectory of its leading vehicle and, therefore, the vehicle needs to decelerate to maintain the spatial-temporal distance determined by the Newell car-following rules. Therefore, at point B (shown in FIGURE 13) the vehicle begins to decelerate, according to the Akçelik deceleration profile. When the driver decelerates at any time earlier than t_B, the resulted trajectory does not intersect with the spatial-temporal shifted trajectory of the vehicle with ID=2.

With this rule, we could numerically determine spatial-temporal point B. Therefore, the new expected departure moment from the stop-line is t_H, which is indicated by point H in the figure. H is the intersection point by the spatial-temporal shifted trajectory of the vehicle with ID 2. However, time t_H is within the red duration and, hence, the vehicle needs to decelerate. At point D, the vehicle decelerates and, at point E, the speed reaches zero while the vehicle is located at the stop-line. When the road speed limit and vehicle maximal deceleration are given, the deceleration profile is fixed. Hence, it is assumed to have been known prior. When green begins, the vehicle accelerates again, according to the Akçelik acceleration profile. From this figure, we can also see that the trajectory of the vehicle consists of several parts: part AB is free flow state, part BC is deceleration state, part CD is obtained by spatial-temporal shifted trajectory, part DE is deceleration profile, part EF is standstill state, and part FK is the acceleration state. Combining the above parts together, the complete trajectory of this vehicle could be revealed. The departing moment for this vehicle is also known by interpolating the trajectory. Note that, if the expected trajectory does not intersect with the spatial-temporal shifted trajectory of its leading vehicle, then the expected trajectory is exactly the ultimate experienced trajectory.

Therefore, given the signals for each cycle (r_1, g_1, r_2, g_2..), the arrival moment of each vehicle, and the vehicle type (HDV, CAV1, or CAV2), the departure profile could be constructed using the method described above. Note that the departure profiles $D_{i,W,TH,HDV}(t)$, $D_{i,W,TH,CAV1}(t)$, and $D_{i,W,TH,CAV2}(t)$ cannot be expressed analytically.

To facilitate the delay calculation, we define the queue length curve $Q_{i,W,TH}(t)$ which is $Q_{i,W,TH}(t) = Q_{i,W,TH,HDV}(t) + Q_{i,W,TH,CAV1}(t) + Q_{i,W,TH,CAV2}(t)$. $Q_{i,W,TH}(t)$ is defined over $N_{i,W,TH}(t)$ and $D_{i,W,TH}(t)$. Its definition is given in:

$$Q_{i,W,TH}(t) = \max\left\{0, N_{i,W,TH}\left(t - \frac{d_{i-1,i}}{\tilde{v}}\right) - D_{i,W,TH}(t)\right\} \tag{6}$$

Similarly, we could also define $Q_{i,W,TH,HDV}(t)$ and $Q_{i,W,TH,CAV1}(t)$ and $Q_{i,W,TH,CAV2}(t)$. Eq. (6) assumes that

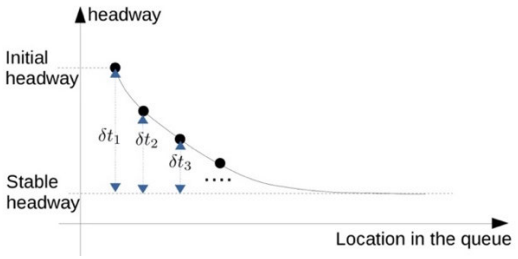

FIGURE 9. Definition and calculation of startup loss.

the moment when one vehicle joins the queue (if there is any) is the expected departure time from the stop-line.

E. MIXED FLOW PLATOON DISPERSION MODELING

This section presents the methodology to solve the second step problem, with the development of a platoon dispersion model to capture the expected arrival profile at downstream intersection i+1, $N'_{i+1,W,CAV}(t)$ and $N'_{i+1,W,HDV}(t)$.

Without a loss of generality, we focus on the western approach through movement at intersection i, *and* western approach through movement at intersection $i+1$, as shown in FIGURE 1, since the two movements are coordinated movements. In the following subsection, we refer to the stop-line of the western approach at intersection i, as the "upstream stop-line", and refer to the stop- line of the western approach at intersection i+1, as the "downstream stop-line". The departure profile at the upstream stop-line is denoted as $D_{i,W,TH}(t)$ while the arrival of the downstream stop-line is denoted as $N'_{i+1,W,TH}(t)$. The departure profile, which is discharged from the stop-line at the western approach through lane experience, a platoon dispersion. The reason for such dispersion is due to the heterogeneity in vehicle speeds. However, the CAVs are controlled by computer algorithms, so their speeds could be accurately controlled. Therefore, there is no dispersion of CAVs, although the dispersion exists for HDVs. The distance between intersections i and i+1 is $d_{i,i+1}$, and the speed limit is v_{max}. We assume that the cumulative departure curve $D_{i,W,TH}(t)$ is known and $D_{i,W,TH}(t) = D_{i,W,TH,HDV}(t) + D_{i,W,TH,CAV1}(t) + D_{i,W,TH,CAV2}(t)$. As the CAVs are assumed to operate at a constant speed v_{max}, we have:

$$\begin{cases} N'_{i+1,W,TH,CAV1}(t) = D_{i,W,TH,CAV1}\left(t - \dfrac{d_{i,i+1}}{v_{max}}\right) (a) \\ N'_{i+1,W,TH,CAV2}(t) = D_{i,W,TH,CAV2}\left(t - \dfrac{d_{i,i+1}}{v_{max}}\right) (b) \end{cases} \quad (7)$$

Eq. (7) indicates that the downstream arrival profile of CAVs is just a temporal shift of the upstream departure curve. For HDVs, we assume that the probability distribution function (PDF) is $f_V(v)$ and the cumulative distribution function (CDF) is $F_V(v)$. For each vehicle that departs, at instance t_0, the distribution of the arrival moment at a downstream stop-line $f_{AT}(t)$ and cumulative distribution $F_{AT,t_0}(t)$ is:

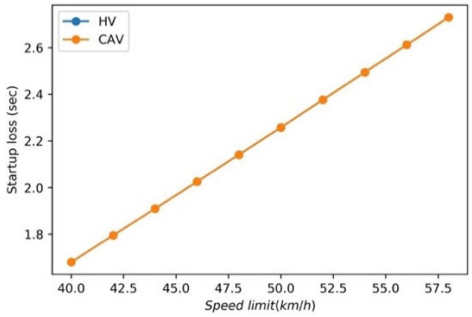

FIGURE 10. Startup loss time versus speed limit.

$$f_{AT,t_0}(t) = p\left(t_0 + \frac{d_{i,i+1}}{v} = t\right) = p\left(v = \frac{d_{i,i+1}}{t - t_0}\right) = f_V\left(\frac{d_{i,i+1}}{t - t_0}\right) \quad (8)$$

$$F_{AT,t_0}(t) = p\left(t_0 + \frac{d_{i,i+1}}{v} < t\right) = p\left(v > \frac{d_{i,i+1}}{t - t_0}\right) = 1 - F_V\left(\frac{d_{i,i+1}}{t - t_0}\right) \quad (9)$$

The departure time of n_{th} vehicle could be expressed as $D^{-1}_{i,W,TH,HDV}(n)$ and, hence, its arrival moment distribution at the downstream stop-line is $f_V(d_{i,i+1}/(t - D^{-1}_{i,W,TH,HDV}(n))$. Note that $D^{-1}_{i,W,TH,HDV}(n)$ could be interpolated from $D_{i,W,TH,HDV}(n)$, which is assumed known. As the arrival moment at the downstream stop-line is random, $N'_{i+1,W,TH,HDV}(t)$ is also random. We use the sum of cumulative arrivals at the downstream stop-line as the predicted cumulative curve $N'_{i+1,W,TH,HDV}(t)$, which could be formulated as:

$$N'_{i+1,W,TH,HDV}(t) = \sum_k F_{AT,D^{-1}_{i,W,TH,HDV}(K),}(t) = \sum_k \left[1 - F_V\left(\frac{d_{i,i+1}}{t - D^{-1}_{i,W,TH,HDV}(k)}\right)\right] \quad (10)$$

It should be noted that the results from Eq. (9) may not have been discrete. Therefore, we need to interpolate the arrival moment for a discrete number of cumulative vehicles. Additionally, the speed distribution of the HDVs needs to be specified. A family of speed distribution models could be used, such as truncated normal speed distribution (Wu *et al.*, [21]) and normal distribution (Pacey, [23]), and the travel time distribution model, such as shifted geometric distribution of travel time, could also be combined. After the downstream arrival of the CAVs and the HDVs is derived, the total arrivals could be calculated as:

$$N'_{i+1,W,TH}(t) = N'_{i+1,W,TH,HDV}(t) + N'_{i+1,W,TH,CAV1}(t) + N'_{i+1,W,TH,CAV2}(t) \quad (11)$$

Next, we show an example of platoon dispersion with different mixed flows, by using the truncated normal speed

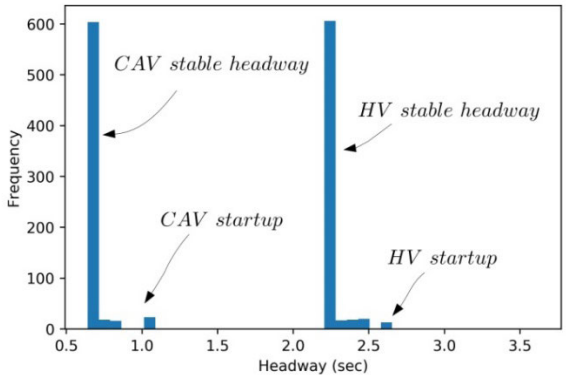

FIGURE 11. Headway histogram without HDV randomness.

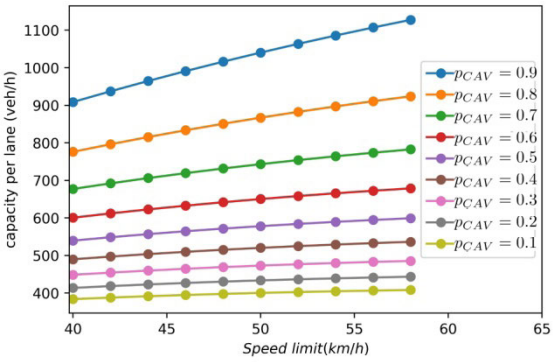

FIGURE 12. Capacity per lane for mixed flows.

distribution in Wu *et al.* [21] as input to the platoon dispersion model. We randomly generate the arrival flows that are given two ratios: HDV ratio p_{HDV} and CAV ratio p_{CAV}. The red duration is set to 500 sec in order to create a long enough queue for discharge. The ratio of $p_{HDV} : p_{CAV}$ is set to 1:9 and 9:1, respectively. The road length is 500m and the minimal, maximal speed is 5m/s and 20m/s, respectively, which is based on the calibration results from Wu *et al.* [21]. FIGURE 14 presents the discharging flow rate and the arrival flow rate at the downstream stop-line (the distance specified above, which is 500m). FIGURE 14(a) illustrates a case when major vehicles are CAV, and FIGURE 14(b) shows a case when major vehicles are HDV. For the same discharging flow[1], arrivals are different for various compositions of vehicles, which lead to different reactions, such as delays, etc.

F. DELAYS AND STOPS CALCULATIONS

Given the cumulative curve, departure curves, and queue curves, the performances index could be formulated. The frequently used PIs include delays, stops, and queues. We have formulated the queue already in Eq. (6). A delay is defined as the difference between the expected travel time and the actual travel time. For the n_{th} vehicle in the arrival sequence, the arrival moment is $N^{-1}_{i,W,TH}(n)$, and the departure moment is $D^{-1}_{i,W,TH}(n)$. As we project the number of vehicle arrivals at the boundary of RSU to the arrivals at the stop-line, the delays could be formulated as $D^{-1}_{i,W,TH}(n) - N^{-1}_{i,W,TH}(n)$. The total number of delays for this specific movement becomes $\sum_j D^{-1}_{i,W,TH}(j) - N^{-1}_{i,W,TH}(j)$, while the total number of delays for intersection i is calculated as:

$$PI_{D,i} = \sum_{\mathcal{A},\mathcal{D}} \sum_{j} D^{-1}_{i,\mathcal{A},\mathcal{D}}(j) - N^{-1}_{i,\mathcal{A},\mathcal{D}}(j), \mathcal{A} \in \{E, W, S, N\}, \mathcal{D} \in \{L, TH, R\} \quad (12)$$

[1]Note that, in order to compare a downstream arrival with the same upstream departure, we set the headways for different leading-following vehicles to 2 sec. This could be seen from the stable vehicles counter of upstream departures. The arrivals were randomly generated by using the mechanism described in Section 3.1.2.

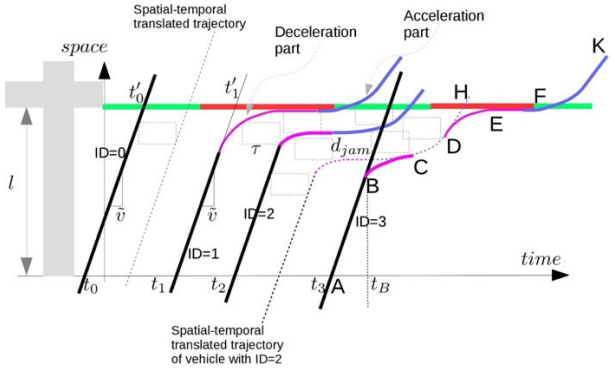

FIGURE 13. The arrival and departure process.

The number of delays for the intersection system is simply the summation over intersections and could be formulated as $PI_D = \sum_i PI_{D,i}$.

The PI of stops is defined as how many stops a vehicle experienced at the signal control horizon–the arrival and departure moments of j_{th} vehicle $N^{-1}_{i,W,TH}(j)$ and $D^{-1}_{i,W,TH}(j)$. There are the following two cases:

1) if $Q_{i,W,TH}\left(N^{-1}_{i,W,TH}(j)\right) = 0$ (which means that there is no queue and, hence, the j_{th} vehicle does not experience any stop);
2) if $Q_{i,W,TH}\left(N^{-1}_{i,W,TH}(j)\right) > 0$ (the arrival and departure times does not belong to the same cycle, so the number of stops that the vehicle experienced depends on a difference in the cycle index of the arrival and departure moments. Define the cycle index function as $\mathcal{K}(t) = k$, $\sum_{i=1}^{k} C_i \le t < \sum_{i=1}^{k+1} C_i$, then the stops for vehicle j are $\mathcal{K}\left(D^{-1}_{i,W,TH}(j)\right) - \mathcal{K}\left(N^{-1}_{i,W,TH}(j)\right) + 1$.

Considering the above two cases, the stops index for the intersection are formulated as:

$$PI_{S,i} = \sum_{\mathcal{A},\mathcal{D}} \sum_{j} Q_{i,\mathcal{A},\mathcal{D}}\left(N^{-1}_{i,\mathcal{A},\mathcal{D}}(j)\right)\left(\mathcal{K}\left(D^{-1}_{i,\mathcal{A},\mathcal{D}}(j)\right) - \mathcal{K}\left(N^{-1}_{i,\mathcal{A},\mathcal{D}}(j)\right) + 1\right) \quad (13)$$

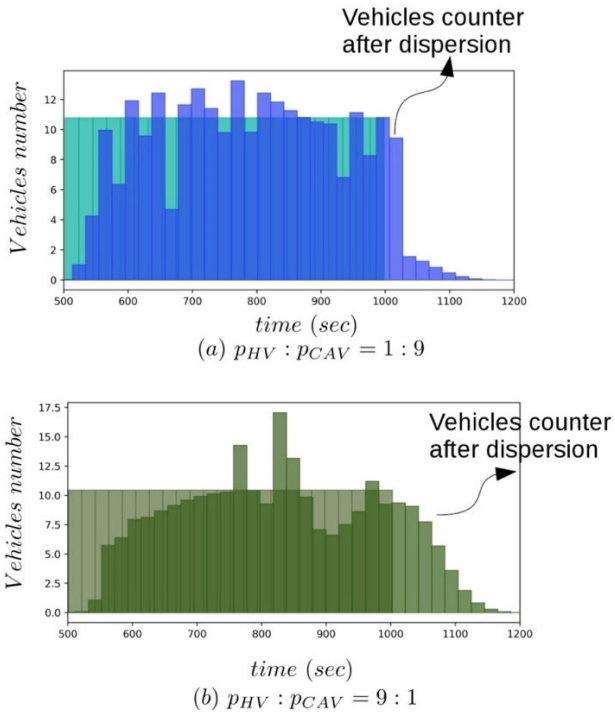

FIGURE 14. Platoon dispersion for different vehicles ratios. The rectangular part is the discharging flow at upstream intersection. And the irregular histogram are the dispersed flow rate at downstream location.

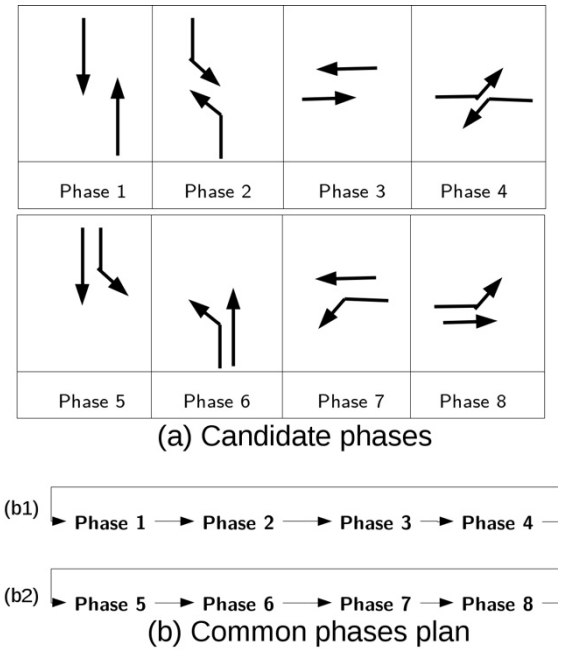

FIGURE 15. Candidate phases and two common phase plans.

Similarly, we have the stops index for the whole intersection coordination systems as $PI_S = \sum_i PI_{S,i}$.

Generally, there are many objectives pursued during the signal optimization. For the intersection coordination, the most used performances include green-wave band width and the delay. Other performances indexes can be easily considered using the parameters set in the above model. For instance, the queue length at moment t is expressed directly by $Q_{i,W,TH}$ (t). With the real-time queue length, the fuel consumption and other emission related PI can be derived indirectly. Thus although we mainly focus on the delay, other PIs are easily to be considered.

G. INTERSECTION SIGNAL SETTINGS

1) CANDIDATE PHASE PLANS

For a common intersection with four legs, there are eight possible phases, as shown in the following figure. The phase plans (phase sequence within a cycle) generally include two types, as given in FIGURE 15(b). The b.1 phase plan is through-left alternative for the south-north bound and for the east-west bound, respectively. On the other hand, the b.2 phase plan serves all movements in just one approach for each phase.

Emerging technologies, such as CAV, have enabled the communication of signal phases and timing (SPaT) information between the infrastructure and vehicles, thereby making flexible phase plans preferred. According to Qi *et al.* [19], based on candidate phases, there are a total of 49 possible phase plans. Plans b.1 and b.2 in FIGURE 15(b) are the two most popular phase configurations, although any plan (among the 49) could have be used.

2) SIGNAL PARAMETER SETTING

The signal optimization of coordinated intersections primarily includes three steps: (1) determining the phase sequences at each intersection; (2) optimizing the cycle length and green duration; and (3) setting the offset.

With regard to the first step, in order to fully utilize the potential of signal control methods, we use the following phase plan configurations:

- Plan b.1, shown in FIGURE 15(b), is set first and, then, the manager optimizes cycle length C and the corresponding green duration.
- The traffic operator does not prefer any phase plan (within the 49 plans), but selects the best one based on some predefined PI, such as delays or capacity;

With regard to the second and third steps of coordinated intersection signal optimizations, we resort to particle swarm optimization techniques, since the underlying traffic flow dynamics is nonlinear. Note that, once the phase sequences are determined, the resulting decision variables (cycle length, green duration, offset) are all continuous variables. They are bounded by minimal green g_{min}, maximal green duration g_{max}. When the cycle length of the intersections is determined, all the coordinated intersections share a common cycle length, the offset range is also determined, which is a positive number that is smaller than that of the common cycle length.

H. COORDINATED SIGNAL OPTIMIZATION MODEL

A model to optimize signal parameters is presented in this section, along with the arrival pattern of each movement as input. Decision variables include the following: cycle length C, duration for each phase g_{p_i} and the offset $o_{ki,i+1}$. We use a modified particle swarm optimization (PSO) to obtain the optimal signal solution. The modified PSO work as follows:

1) Set PSO parameters: the maximal iteration N_{Iter}, particles number $N_{particle}$ and maximal velocity S_{max};
2) Set iteration counter $Iter = 0$, and randomly drew a green duration and cycle length, as follows: a) uniformly drew green durations $G' = \{g'_{p11}, g'_{p12} \ldots g'_{p21}, g'_{p22} \ldots .o'_{1,2}, o'_{2,3}.., \}\forall$ I, j for each phase p_{ij}. The phase p_{ij} is the j_{th} phase of intersection i, and $o_{i,i+1}$ is the offset of intersection i+1 with respect to intersection i. The cycle length at intersection i, then, is $C'_i = t_{loss}n_{p_{ij}} + \sum_i g'_{p_{ij}}$, where $n_{p_{ij}}$ is the number of phases for intersection i. b) As all intersections share the same cycle length, the common cycle length is $C' = \max(C'_i)$. c) As the sum of all phase durations could exceed the cycle length C_{max}, i.e. $C' > C_{max}$, the transformed cycle length is, as follows: $C = \max\{C_{max}, C'\}$. d) Calculate the green duration for each phase using $g_{p_{ij}} = [C - t_{loss}n_{p_{ij}}]g'_{p_{ij}} / \sum_i g'_{p_{ij}}$, and also got the offset $o_{i,i+1} = \min\{\max\left\{0, o'_{i,i+1}\right\}, C\}$. e) Repeat the above procedures and got $N_{particle}$ particles G_j, j = 1, 2, ...$N_{particle}$. f) Then, compute the performance index (either delays or stops, or both) for each particle G_j, and indicate the above populations during iteration *Iter* as G(*Iter*);
3) For each particle in $G_j(Iter)$, the historical best solution chosen is $\hat{G}_j$ and the global best of Iter is $\hat{G}$. The above two variables are updated during each iteration;
4) Calculate the velocity $\mathbb{S}_j$ of each particle G_j using $\mathbb{S}_j(Iter + 1) = w\mathbb{S}_j(Iter) + c_1(\hat{G}_j - G_j(Iter)) + c_2(\hat{G} - G_j(Iter))$; update the candidate solution, using $G'_j(Iter + 1) = G_j(Iter) + min(\mathbb{S}_j(Iter + 1), \mathbb{S}_{max})$; after that. use steps 2.b ~d to get the $G_j(Iter + 1)$;
5) If N_{Iter} is not reached, returned to step (3);

During the above process, if the candidate $G_j(Iter)$ becomes infeasible (when green duration exceeds the minimal and maximal boundaries), a large penalty is imposed on the performance index. The parameters are set as follows: $w = 0.5$, $c_1 = 0.5$ and $c_2 = 0.5$.

III. EXPERIMENT STUDY

A. SCENARIOS SETUP

As field data collection and experiment implementation is not yet possible due to the lack of CAV real-world deployment, real-world intersections were used as a target study area, with simulated demand settings giving the field detected flow rates. We selected two intersections in Hang Zhou, China to validate the proposed algorithm. The two intersections were XiHu Rd-Zhonghe Rd and Xi Rd-Yanan Rd (FIGURE 16 a and b). The geometry and the detectors are shown in the following figure:

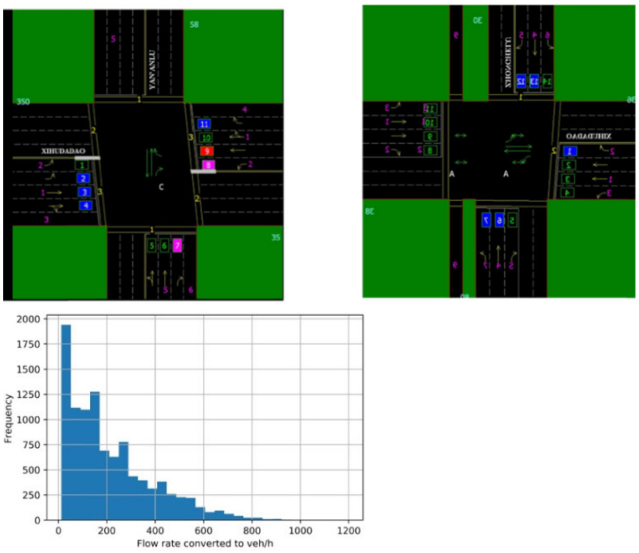

FIGURE 16. Scenario Setup: (a) XHu Rd-Yanan Rd, (b) XiHu Rd-Zhonghe Rd, (c) The hourly flow rate.

The distance between the two intersections was 712 m. Right-turn movements were not controlled and, thus, not considered. The detector output at the intersection was at a 5 min-flow rate (shown in FIGURE 16c), which was an aggregate of all detector data. This showed that there was no apparent transition between flow rates. Therefore, we set three levels of flow rate or demand levels–low, medium, and high–which corresponded to 200veh/h, 400 veh/h, and 600veh/h, respectively. Note that the flow rate was defined for one lane. There was a total of 16 movements, and the flow rate of each movement needed to be defined. An experiment, hence, could be carried out by sampling the demand, given the flow rate. The sampling of the movement of a specific flow is given in the follow section.

The speed limit of the selected road was 50km/h, which was a common speed limit for an urban road network in China. The upper and lower boundaries of the speed limit, used in the platoon dispersion component, was 5m/s and 20m/s, or 18 km/h and 72 km/h.

1) BENCHMARK SIGNAL PLAN A

To analyze the results of our method, we chose a common signal setting method as the first benchmark. We assumed that the signal phases were given, (i.e., plan b1 in FIGURE 15). The phases were labeled as $\{p_1, p_2, p_3 \ldots .p_n\}$. The arrival flow rate for each phase (if there more movements in one phase, we chose the maximal one) were $\{q_{p_1}, q_{p_2}, q_{p_3} \ldots .q_{p_n}\}$. We assumed the saturation flow rate was S=1800veh/h, and the cycle length was calculated as $C = \min\{nt_{loss}/(1 - \sum_i q_{p_i}/s), C_{max}\}$. This method was documented in HCM [20] and was applied extensively. The green duration for each phase was calculated as

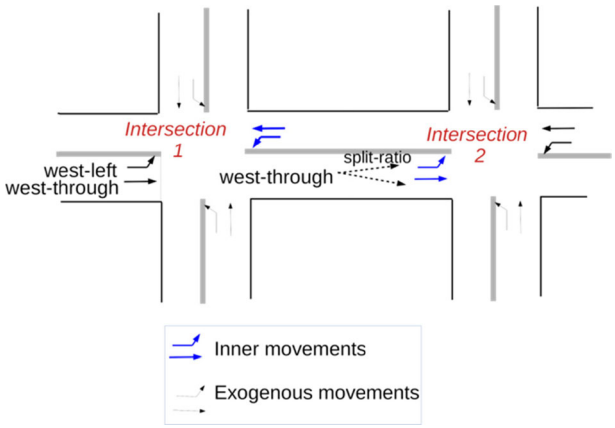

FIGURE 17. Demand settings for coordinated intersections experiment.

$g_{p_i} = (C - nt_{loss})(q_{p_i}/s)/\sum_i (q_{p_i}/s)$. Given the signal plans and duration of each intersection, the greatest cycle length was then applied to all coordinated intersections. The next step was to find the offset between intersections. The MAXBAND method was used to calculate the best offset, which tried to maximize the weight sum of the two-direction bandwidths. As the cycle length and the green split were set and the speed limit was assumed to have been fixed, they could be easily inferred in the MAXBAND.

2) BENCHMARK SIGNAL PLAN B

Based on the analysis of capacity in mixed traffic flow, it was found that the resulting headways were drastically different from the pure HDV scenario. Therefore, benchmark signal plan B was set up to test the improvements brought by a more accurate saturation flow rate S with formula $C = \min\{nt_{loss}/(1 - \sum_i q_{p_i}/s), C_{max}\}$. Note that we had found that the lost time was identical for both types of vehicle. As the saturation flow rate was the reciprocal of a stale headway, we could use the stable headway for different types of vehicle, as a start. The stable headway was expressed as $h = \tau + d_{jam}/v_f$. Using τ_{HDV} and τ_{CAV}, we had stable headways, h_{HDV} and h_{CAV}. Suppose the ratio of HDV was π_{HDV}, then the weighted saturation flow rate could have been computed as $S' = \pi_{HDV}(3600/h_{HDV}) + (1 - \pi_{HDV})(3600/h_{HDV})$. Therefore, the cycle length became $C = \min\{nt_{loss}/(1 - \sum_i q_{p_i}/S_{p_i}), C_{max}\}$, where S_{p_i} was the weighted saturation flow rate. The split and the offset could be calculated using the same method as in benchmark plan A.

3) DEMAND SETTING

The demands were the directional flow rate, or arrival flow rate. As shown in the following figure, there were two intersections. As the right-turn flows were generally not controlled, we omitted the right-turn movement and only dealt with left-turn and through movement. There was a total of 16 movements (8*2), 8 for each intersection. Four of these movements were determined by the upstream departures, which were then controlled by a coordinated signal. These four movements (labeled in blue in FIGURE 17) were named "inner movements". The arrival flows of inner movements were obtained by splitting departures from the upstream stop-line. We assumed a equal split ratio for each departing movement, i.e., the split ratio of the west-through movement in FIGURE 17 was 0.5-0.5 (the right turn flow was omitted since it was not controlled by the coordinated signal). Other movements (12), named "exogenous movements" were set as follows, with three levels of flow rate used–200veh/h, 400veh/h, and 600veh/h.

There was a total of 3^{12} combinations (recall that we had 12 movements), which was a huge number. Hence, we used orthogonal experimental design to set the arrival flow rates. Taguchi orthogonal Array was employed for this purpose. As there were three levels, we could adopt a L27(3^{13}) array. This meant that there were 27 combinations that could accommodate 13 factors. As we only had 12 movements, the last column could be omitted. The orthogonal array is given in Appendix A.

For each movement, we generated the vehicle arrivals, based on the following parameters:

- There were three types of vehicle arrivals: HDV, CAV1, and CAV2. The last type was a batch arrival, i.e., there was more than one vehicle with smaller headway h_{CAV2};
- The interval between any two types of arrival was random and interdependent, so we used ξ to indicate the interval between neighboring arrival modes and $f_\xi(t)$ to indicate the distribution of the interval;
- The arrival type was independent of the historical arrival mode, including its leading arrival mode. We used an arrival mode matrix $\pi = [\pi_{HDV}, \pi_{CAV1}, \pi_{CAV2}]$ to indicate the dependence probability. π_{HDV} was the probability that the arrival mode was human-driven vehicles;
- For the last arrival type (CAV2), we used a Poisson distribution to indicate the batch number. Thus, there would be another parameter ϕ, which was the mean number of arrivals for CAV2.

Therefore, after specifying the interval distribution $f_\xi(t)$, arrival mode vector π and ϕ, we were ready to draw samples from the mixed process and take the samples as the input demand. Given the three inputs, the mean number of vehicle arrivals, or the flow rate, the calculation could be:

1) First, obtain the mean of the interval $E(\xi)$;
2) The probability that the arrival mode was CAV2 was π_{CAV2}, and the mean arrival vehicles was ϕ. Therefore, the time duration for these vehicles was $E(\xi) + \phi h_{CAV}$, and the flow rate for mode CAV2 was $\phi/(E(\xi) + \phi h_{CAV2})$;
3) Therefore, the mean flow rate was $\pi_{HDV}/E(\xi) + \pi_{CAV1}/E(\xi) + \pi_{CAV2}\phi/(E(\xi) + \phi h_{CAV})$

We used the logic above to sample the vehicles arrivals (including its type, i.e., HDV, CAV1, or CAV2), input arrivals to the system, optimize the signal, and output the results.

In order to investigate the influence of different proportions of vehicles, for each flow rate q, we set three

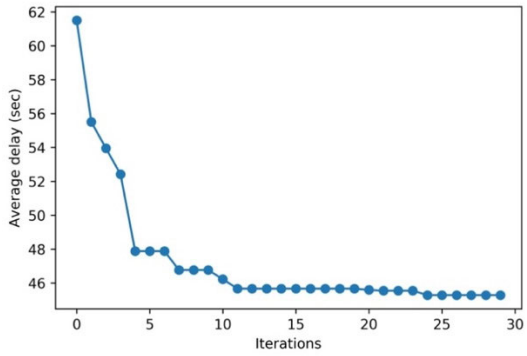

FIGURE 18. The convergence of the PSO algorithm.

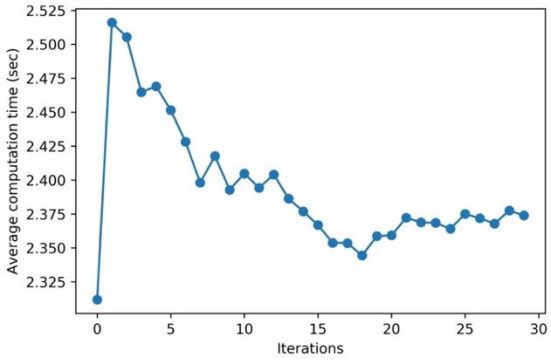

FIGURE 19. Average time consumption of each iteration.

types of proportion as follows: (1) HDV:CAV1:CAV2=1:1:8, i.e. $\pi = [0.1, 0.1, 0.8]$; (2) $\pi = [0.1, 0.8, 0.1]$; (3) $\pi = [0.8, 0.1, 0.1]$. For easy reference purposes, we indicated the above three ratio settings as Π_1, Π_2 and Π_3. In the equation $q = \pi_{HDV}/E(\xi) + \pi_{CAV1}/E(\xi) + \pi_{CAV2}\phi/(E(\xi) + \phi h_{CAV2})$, when q and π were specified, there were two unknown variables: ϕ and $E(\xi)$. When ϕ was 2, $E(\xi)$ could be solved from the above equation. It meant that the CAV2 type vehicles arrived in a batch manner, and the mean vehicle batch size was 2. Because there were 27 plans for experiment on flow rate levels, and we had 3 types of flow compositions, we needed to carry out experiments for 81 (27∗3) demand types in total. For each demand type, we optimized the signal using the PSO and benchmark methods.

B. EXPERIMENT RESULTS

1) ALGORITHM COMPUTATIONAL EFFICIENCY

We initially investigated the model convergence. FIGURE 18 and FIGURE 19 give the convergence and the computational efficiency of the proposed PSO algorithm. The algorithm was coded on a common laptop with Intel®Core™i5-7300U Processor and 16GB RAM. The particles number was set to be 100, and the algorithm was coded in python and tested by Anaconda, a scientific oriented package. FIGURE 18 shows the results when the delay minimization was the objective. The delay was the average delay of all vehicles. It was shown that, in the first few iterations, the delays decreased significantly, whereas, after the10th iteration, the average delay (which was historically the best) did not change very much. Compared with the average delay (about 62 sec/veh) that had been generated by initial random signals, this value reached about 45 sec, which meant that after 10 iterations, the solution outperformed the initial plan by reducing delays by about 25%. FIGURE 19 shows that it takes about 2.5 sec for one iteration. Thus, the time for 20 iterations was within 1 minute. Given that the demand did not change very much during a short interval, and the algorithm implementation could be improved by lower level language, such as C++, this computational efficiency was acceptable for real-time deployment.

2) ALGORITHM PERFORMANCES

For each flow level in TABLE 3 in Appendix A, we sampled the flow rate, according to the demand setting, based on the ratio of each type of vehicle, and then optimized the signals using the proposed PSO method. We used the same demand inputs to optimize the signal, using benchmark plans A and B. For the two plans, we assumed that the phase sequences were b1 in FIGURE 15. As we had 27 demand levels and 3 ratios of vehicle types, there were 81 combinations. TABLE 1 summarizes the results of the 81 combinations comparison between the PSO and benchmark plan A. The column "Bhmk A Π_1" meant that data for this column were the results of benchmark signal plan A, using the ratio $\pi = [0.1, 0.1, 0.8]$. Row field "Demand 1" meant "Demand level 1" and was the 1st row in TABLE 3. The value "40.81" was the delay per vehicle that resulted from the signal plan.

It was observed that, under the same ratio and demand level, the proposed PSO algorithm could always find a plan that had better performance. Under the same demand level, the delays varied for different ratios. The HDVs ratio in Π_1 was 0.1, hence only 10% of the coming vehicles were driven by humans. The CAV2 type was 0.8 and, hence, 80% of the vehicles were CAVs in a platoon mode. Therefore, under ratio Π_1, the delay was minimal, as compared with other two ratios.

For instance, column "PSO Π_1" row "Demand level 1" had a delay of 9.77s, which was smaller than "PSO Π_2" and PSO Π_3. Also, we found that delays may not have increased with the arrival flow rate, due to the fact that, when the flow rate increased, more CAVs in the coming flow reduced the headway and increased the capacity, so that the delay decreased. This could also be revealed from the fact that the column values had not increased. Another reason may have been that the optimization in TABLE 1 had been implemented upon the arrivals. Random generation of different demands, thus lead to different results, which could be analyzed later.

Improvement was calculated as (benchmark delay −PSO delay)/benchmark delay ∗ 100%. FIGURE 20 presents the results. The PSO performed better under every demand level, and for each flow ratio. The maximum improvement was about 70% while the minimal improvement

TABLE 1. Comparison of the delays in 27 experiments, unit is SEC/VEH.

	Bhmk A Π_1	*Bhmk A* Π_2	*Bhmk A* Π_3	*PSO* Π_1	*PSO* Π_2	*PSO* Π_3
Demand 1	40.81	42.78	42.27	9.77	11.54	9.91
Demand 2	52.55	60.36	58.61	34.27	35.39	40.10
Demand 3	62.78	87.03	90.44	38.80	48.68	62.26
Demand 4	56.03	59.77	51.25	34.24	37.92	42.74
Demand 5	63.98	92.34	69.98	37.49	49.28	54.29
Demand 6	53.50	69.29	62.93	35.59	50.35	48.59
Demand 7	59.54	83.43	85.06	43.82	51.69	70.03
Demand 8	55.10	74.38	76.53	35.78	58.52	60.31
Demand 9	59.58	83.65	71.29	33.26	64.04	58.40
Demand 10	54.86	64.59	68.23	34.72	46.77	48.47
Demand 11	53.59	65.75	70.60	38.64	39.17	55.21
Demand 12	55.22	64.89	67.70	38.36	55.68	56.33
Demand 13	60.57	78.08	73.79	38.16	61.09	44.34
Demand 14	52.22	70.45	77.88	34.80	51.69	45.05
Demand 15	60.73	69.44	93.09	35.83	40.35	53.01
Demand 16	53.52	68.02	70.55	31.37	52.77	56.17
Demand 17	56.53	60.82	69.47	34.78	51.23	54.30
Demand 18	43.58	76.03	52.64	39.63	47.10	45.58
Demand 19	55.22	69.10	77.12	36.85	54.57	48.48
Demand 20	56.85	74.01	79.47	38.60	50.03	60.57
Demand 21	60.03	69.62	80.50	38.21	45.23	37.59
Demand 22	59.85	78.10	82.90	41.20	59.50	67.35
Demand 23	54.05	58.39	70.92	38.57	55.71	59.56
Demand 24	53.59	69.22	64.60	38.06	54.58	52.41
Demand 25	53.85	74.40	74.93	36.10	50.06	44.41
Demand 26	58.17	73.56	75.38	35.40	51.26	56.68
Demand 27	57.17	69.10	87.12	39.70	49.73	47.48

was 3%. On average, the proposed method could improve 35% under Π_1, 30% under Π_2, and 28% under Π_3.

We also found that, by using weighted saturation flow rate in the PI was improved. The results were given in TABLE 2. The difference between benchmark plans A and B was that the latter used the weighted saturation flow rate, which was determined by the ratio of HDVs and CAVs. By comparing TABLE I and TABLE 2, we found that, by adjusting the SFR (saturation flow rate) based on arrival demands, a better PI could be achieved. For instance, when using the 1st row demand level in Appendix A and the ratio was set to be Π_1, the delay was 27.11 sec. Compared with the 40.81 sec for benchmark plan A, the result was improved by 13 sec.

The improvement, by adjusting the SFR, could be calculated by using (benchmark A delay − benchmark B delay)/ benchmark A delay. By simply changing the SFR settings, significant achievement could be realized, as shown in

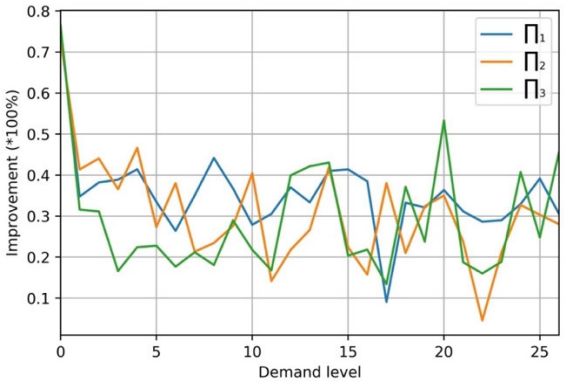

FIGURE 20. Improvement by percentage.

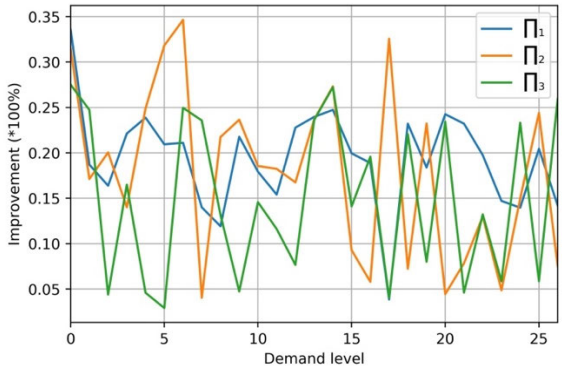

FIGURE 21. Delay improvement by adjusting SFR.

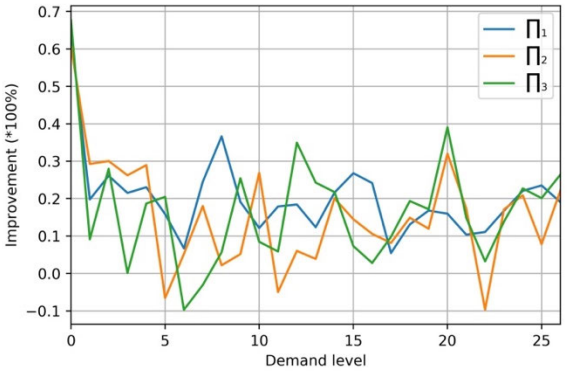

FIGURE 22. Delay improvements by comparing PSO results and benchmark plan B.

FIGURE 21. The minimum improvement was about 5%, while the maximal improvement was 30%. On average, it was estimated that the improvement was about 15%, with varying results for different demand levels and ratios.

Using the results in TABLE 1 and TABLE 2, we could calculate the difference between the PSO and benchmark plan B (improvements were shown in FIGURE 22). These results showed that PSO was generally more favorable, since 77 cases (of 81 cases) outperformed benchmark plan B. The maximum improvement was about 60%. On average,

TABLE 2. Results for benchmark plan B.

	Bhmk B Π_1	*Bhmk B* Π_2	*Bhmk B* Π_3
Demand 1	27.11	29.31	30.64
Demand 2	42.72	50.02	44.11
Demand 3	52.49	69.59	86.45
Demand 4	43.63	51.40	42.80
Demand 5	48.71	69.34	66.76
Demand 6	42.29	47.24	61.10
Demand 7	46.97	54.53	63.83
Demand 8	47.38	71.37	58.49
Demand 9	52.48	65.47	61.90
Demand 10	42.92	49.32	65.00
Demand 11	43.98	53.55	60.31
Demand 12	46.71	53.05	59.84
Demand 13	46.77	65.00	68.13
Demand 14	39.71	53.77	59.49
Demand 15	45.71	50.47	67.74
Demand 16	42.85	61.70	60.59
Demand 17	45.85	57.28	55.86
Demand 18	41.91	51.27	50.52
Demand 19	42.40	64.10	60.11
Demand 20	46.39	56.82	73.11
Demand 21	45.47	66.52	61.65
Demand 22	45.96	71.97	79.08
Demand 23	43.37	50.80	61.54
Demand 24	45.71	65.85	60.81
Demand 25	46.33	63.26	57.45
Demand 26	46.28	55.61	70.95
Demand 27	49.04	63.89	64.53

a 10%∼20% improvements could have been expected while, in only 4 of the 81 cases, did the PSO perform worse than the benchmark case did. Differences were all within 10%.

As arrivals were random, even under the same demand levels, i.e., for the demand level defined by the 4$^{\text{th}}$ row in TABLE 3, using the ratio settings $\pi = [0.1, 0.8, 0.1]$, each incoming vehicle had a time interval that was different from that of the other vehicles, Monte Carlo simulation was carried out, under the same demand level, by using the 4$^{\text{th}}$ row values in TABLE 3 and $\pi = [0.1, 0.8, 0.1]$. It meant that the HDVs accounted for only 10 percent of the flow rate. During each Monte Carlo simulation, we generated the vehicle arrivals, optimized the signals by using the PSO algorithm and compared it with the benchmark plan A.

FIGURE 23 and FIGURE 24 present the results from 50 simulations. FIGURE 23 was the delay histogram for two signal plans—the PSO generated plan and the benchmark plan. It was shown that the average delay spanned from 35 sec

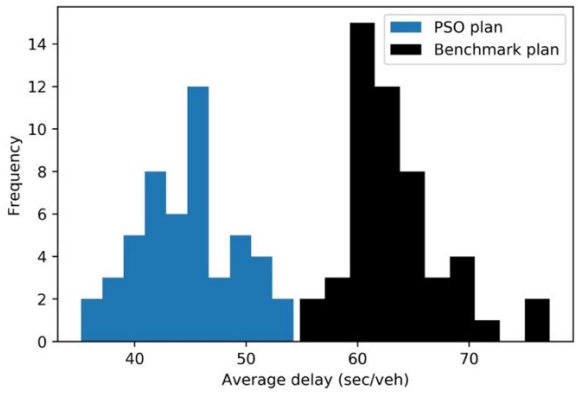

FIGURE 23. Comparison of results for PSO optimization and benchmark plan A.

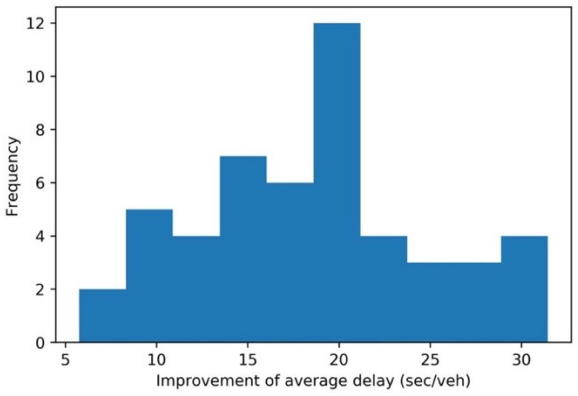

FIGURE 24. The delay improvement from Monte Carlo simulation.

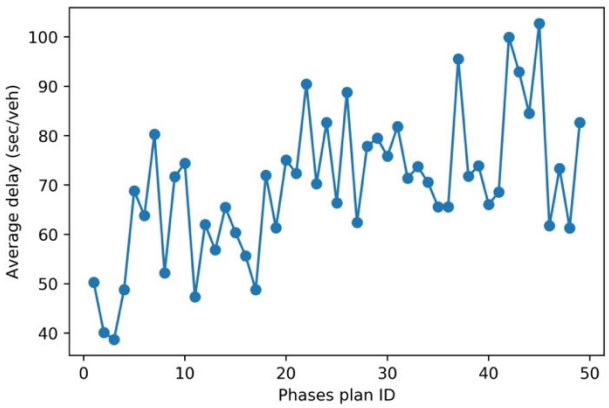

FIGURE 25. Performances by setting different phase plans.

to 55 sec by the PSO plan, whereas this value spanned from 55 sec to 80 sec for the benchmark plan A. It could be concluded that the proposed method could generate better outcomes when the arrivals were random. FIGURE 24 shows the delay improvement by the PSO plan, as compared to that of benchmark. The average improvement was found to be 20.633 sec, whereas the minimum and maximum improvements were 5.75 sec and 35.4 sec, respectively.

TABLE 3. Demand settings which employs taguchi orthogonal design array.

	1	2	3	4	5	6	7	8	9	10	11	12	13	14
1,west	2	2	2	2	2	2	2	2	2	4	4	4	4	4
_throu	0	0	0	0	0	0	0	0	0	0	0	0	0	0
gh	0	0	0	0	0	0	0	0	0	0	0	0	0	0
1,west	2	2	2	4	4	4	6	6	6	2	2	2	4	4
_left	0	0	0	0	0	0	0	0	0	0	0	0	0	0
	0	0	0	0	0	0	0	0	0	0	0	0	0	0
1,sout	2	2	2	4	4	4	6	6	6	4	4	4	6	6
h_left	0	0	0	0	0	0	0	0	0	0	0	0	0	0
	0	0	0	0	0	0	0	0	0	0	0	0	0	0
1,nort	2	2	2	4	4	4	6	6	6	6	6	6	2	2
h_thro	0	0	0	0	0	0	0	0	0	0	0	0	0	0
ugh	0	0	0	0	0	0	0	0	0	0	0	0	0	0
1,sout	2	4	6	2	4	6	2	4	6	2	4	6	2	4
h_thro	0	0	0	0	0	0	0	0	0	0	0	0	0	0
ugh	0	0	0	0	0	0	0	0	0	0	0	0	0	0
1,nort	2	4	6	2	4	6	2	4	6	4	6	2	4	6
h_left	0	0	0	0	0	0	0	0	0	0	0	0	0	0
	0	0	0	0	0	0	0	0	0	0	0	0	0	0
2,east	2	4	6	2	4	6	2	4	6	6	2	4	6	2
_throu	0	0	0	0	0	0	0	0	0	0	0	0	0	0
gh	0	0	0	0	0	0	0	0	0	0	0	0	0	0
2,	2	4	6	4	6	2	6	2	4	2	4	6	4	6
south_	0	0	0	0	0	0	0	0	0	0	0	0	0	0
left	0	0	0	0	0	0	0	0	0	0	0	0	0	0
2,east	2	4	6	4	6	2	6	2	4	4	6	2	6	2
_left	0	0	0	0	0	0	0	0	0	0	0	0	0	0
	0	0	0	0	0	0	0	0	0	0	0	0	0	0
2,nort	2	4	6	4	6	2	6	2	4	6	2	4	2	4
h_thro	0	0	0	0	0	0	0	0	0	0	0	0	0	0
ugh	0	0	0	0	0	0	0	0	0	0	0	0	0	0
2,sout	2	4	6	6	2	4	4	6	2	2	4	6	6	2
h_thro	0	0	0	0	0	0	0	0	0	0	0	0	0	0
ugh	0	0	0	0	0	0	0	0	0	0	0	0	0	0
2,nort	2	4	6	6	2	4	4	6	2	4	6	2	2	4
h_left	0	0	0	0	0	0	0	0	0	0	0	0	0	0
	0	0	0	0	0	0	0	0	0	0	0	0	0	0

TABLE 4. continued.

	15	16	17	18	19	20	21	22	23	24	25	26	27
1,west_t	4	4	4	4	6	6	6	6	6	6	6	6	6
hrough	0	0	0	0	0	0	0	0	0	0	0	0	0
	0	0	0	0	0	0	0	0	0	0	0	0	0
1,west_le	4	6	6	6	2	2	2	4	4	4	6	6	6
ft	0	0	0	0	0	0	0	0	0	0	0	0	0
	0	0	0	0	0	0	0	0	0	0	0	0	0
1,south_l	6	2	2	2	6	6	6	2	2	2	4	4	4
eft	0	0	0	0	0	0	0	0	0	0	0	0	0
	0	0	0	0	0	0	0	0	0	0	0	0	0
1,north_	2	4	4	4	4	4	4	6	6	6	2	2	2
through	0	0	0	0	0	0	0	0	0	0	0	0	0
	0	0	0	0	0	0	0	0	0	0	0	0	0
1,south_t	6	2	4	6	2	4	6	2	4	6	2	4	6
hrough	0	0	0	0	0	0	0	0	0	0	0	0	0
	0	0	0	0	0	0	0	0	0	0	0	0	0
1,north_l	2	4	6	2	6	2	4	6	2	4	6	2	4
eft	0	0	0	0	0	0	0	0	0	0	0	0	0
	0	0	0	0	0	0	0	0	0	0	0	0	0
2,east_th	4	6	2	4	4	6	2	4	6	2	4	6	2
rough	0	0	0	0	0	0	0	0	0	0	0	0	0
	0	0	0	0	0	0	0	0	0	0	0	0	0
2,south_l	2	6	2	4	2	4	6	4	6	2	6	2	4
eft	0	0	0	0	0	0	0	0	0	0	0	0	0
	0	0	0	0	0	0	0	0	0	0	0	0	0
2,east_le	4	2	4	6	6	2	4	2	4	6	4	6	2
ft	0	0	0	0	0	0	0	0	0	0	0	0	0
	0	0	0	0	0	0	0	0	0	0	0	0	0
2,north_	6	4	6	2	4	6	2	6	2	4	2	4	6
through	0	0	0	0	0	0	0	0	0	0	0	0	0
	0	0	0	0	0	0	0	0	0	0	0	0	0
2,south_t	4	4	6	2	2	4	6	6	2	4	4	6	2
hrough	0	0	0	0	0	0	0	0	0	0	0	0	0
	0	0	0	0	0	0	0	0	0	0	0	0	0
2,north_l	6	6	2	4	6	2	4	4	6	2	2	4	6
eft	0	0	0	0	0	0	0	0	0	0	0	0	0
	0	0	0	0	0	0	0	0	0	0	0	0	0

*the unit in the table is veh/h

*the row field "1,west_through" indicates the demand for west approach, through movement at the first intersection; and column field "1" means the first combination

According to Qi *et al.* [19], there were a total of 49 phase sequences for a typical four-leg intersection. For each plan, we optimized the cycle lengths and green durations. The average delays for different phase plans are shown in FIGURE 25. The first plan (with id = 1) corresponded to plan b2 in FIGURE 15. The phase plan with id=4 corresponded to plan b1 in FIGURE 15, which was also the default plan in TABLE 1. It could be observed that various phase sequences led to different performances. The resulting delay spans were from 40 sec/veh to about 100 sec/veh. The phase sequence, with the best performance, was found to be the third plan. Compared with the default plan, i.e., b1 in FIGURE 15, the best plan reduced the delay by about 10 sec/veh.

IV. CONCLUSION AND REMARKS

Advancements in connected and autonomous vehicle technologies have brought challenges to the modern-day traffic control system which has been designed for HDVs only. The difference between CAVs and HDVs is that the former behaves accurately, while the latter is random in nature due to differences in human driving behavior that include speed, headways, etc. This manuscript investigated coordinated intersection signal design problem for mixed traffic flows of Human-Driven Vehicles (HDVs) and Connected and Autonomous Vehicles (CAVs). Three locations, namely entrance location where the loop detector was located at, and upstream intersection and downstream intersection were defined. Two types of vehicle cumulative curves, namely cumulative arrival profile and cumulative departure profile were constructed.

The mixed-flow traffic dynamics were analyzed, and the arrival-departure curves relationship was derived using a combination of Newell car-following and Akçelik acceleration model. A mixed-flow platoon dispersion model was proposed to describe the vehicle's progression between two locations. Due to the nonlinear nature of the problem, a particle swarm optimization (PSO) method was employed to obtain the optimal signal parameters, including the cycle length, green duration, and optimal offset. The algorithm was implemented and validated in a case study involving two intersections, with the demand formulated and simulated by the Markov chain. The results showed that the proposed model could effectively decrease delays when compared with current signal control methods.

APPENDIX A

See Table 3.

REFERENCES

[1] R. Akçelik and M. Besley, "Acceleration and deceleration models," in *Proc. 23rd Conf. Austral. Institutes Transp. Res. (CAITR)*, Melbourne, VIC, Australia: Monash Univ., 2001, p. 12.

[2] B. Beak, K. L. Head, and Y. Feng, "Adaptive coordination based on connected vehicle technology," *Transp. Res. Rec.*, vol. 2619, no. 1, pp. 1–12, Jan. 2017.

[3] K. C. Dey, L. Yan, X. Wang, Y. Wang, H. Shen, M. Chowdhury, L. Yu, C. Qiu, and V. Soundararaj, "A review of communication, driver characteristics, and controls aspects of cooperative adaptive cruise control (CACC)," *IEEE Trans. Intell. Transp. Syst.*, vol. 17, no. 2, pp. 491–509, Feb. 2016.

[4] N. H. Gartner, C. J. Messer, and A. Rathi, "Traffic flow theory-a state of the art report: Revised monograph on traffic flow theory," FHWA, Washington, DC, USA, 2002.

[5] Y. Guo, J. Ma, C. Xiong, X. Li, F. Zhou, and W. Hao, "Joint optimization of vehicle trajectories and intersection controllers with connected automated vehicles: Combined dynamic programming and shooting heuristic approach," *Transp. Res. C, Emerg. Technol.*, vol. 98, pp. 54–72, Jan. 2019.

[6] K. Dresner and P. Stone, "A multiagent approach to autonomous intersection management," *J. Artif. Intell. Res.*, vol. 31, pp. 591–656, Jul. 2018.

[7] H. Hao and W. Ma, "Revisiting distribution model of departure headways at signalised intersections," *Transportmetrica B, Transp. Dyn.*, vol. 5, no. 1, pp. 1–14, Jan. 2017.

[8] M. Hausknecht, T.-C. Au, and P. Stone, "Autonomous intersection management: Multi-intersection optimization," in *Proc. IEEE/RSJ Int. Conf. Intell. Robots Syst.*, Sep. 2011, pp. 4581–4586.

[9] J. D. C. Little, M. D. Kelson, and N. H. Gartner, "MAXBAND: A versatile program for setting signals on arteries and triangular networks," *Transp. Res. Rec.*, vol. 759, pp. 40–46, Jan. 1981.

[10] J. Lioris, R. Pedarsani, F. Y. Tascikaraoglu, and P. Varaiya, "Platoons of connected vehicles can double throughput in urban roads," *Transp. Res. C, Emerg. Technol.*, vol. 77, pp. 292–305, Apr. 2017.

[11] X. Jin, Y. Zhang, F. Wang, L. Li, D. Yao, Y. Su, and Z. Wei, "Departure headways at signalized intersections: A log-normal distribution model approach," *Transp. Res. C, Emerg. Technol.*, vol. 17, no. 3, pp. 318–327, Jun. 2009.

[12] J. Lee, B. B. Park, K. Malakorn, and J. J. So, "Sustainability assessments of cooperative vehicle intersection control at an urban corridor," *Transp. Res. C, Emerg. Technol.*, vol. 32, pp. 193–206, Jul. 2013.

[13] L. Li and X. M. Chen, "Vehicle headway modeling and its inferences in macroscopic/microscopic traffic flow theory: A survey," *Transp. Res. C, Emerg. Technol.*, vol. 76, pp. 170–188, Mar. 2017.

[14] V. Milanes, S. E. Shladover, J. Spring, C. Nowakowski, H. Kawazoe, and M. Nakamura, "Cooperative adaptive cruise control in real traffic situations," *IEEE Trans. Intell. Transp. Syst.*, vol. 15, no. 1, pp. 296–305, Feb. 2014.

[15] A. Mirheli, L. Hajibabai, and A. Hajbabaie, "Development of a signal-head-free intersection control logic in a fully connected and autonomous vehicle environment," *Transp. Res. C, Emerg. Technol.*, vol. 92, pp. 412–425, Jul. 2018.

[16] *U.S. Department of Transportation Releases Policy on Automated Vehicle Development*, U.S. Dept. Transp., Nat. Highway Traffic Saf. Admin., Washington, DC, USA, 2013.

[17] Ni, Daiheng, "Extension and generalization of Newell's simplified theory of kinematic waves," Ph.D. dissertation, Georgia Inst. Technol., Atlanta, GA, USA, 2004.

[18] J. Ploeg, B. T. M. Scheepers, E. Van Nunen, N. Van De Wouw, and H. Nijmeijer, "Design and experimental evaluation of cooperative adaptive cruise control," in *Proc. 14th Int. IEEE Conf. Intell. Transp. Syst. (ITSC)*, Oct. 2011, pp. 260–265.

[19] H. Qi, Y. Ye, J. Xu, and D. Wang, "Intersection control considering channelized section spillback using a flexible phase plan," *J. Transp. Eng.*, vol. 142, no. 1, Jan. 2016, Art. no. 04015032.

[20] *Highway Capacity Manual*. Transportation Research Board, Nat. Res. Council, Washington, DC, USA, 2010.

[21] W. Wu, L. Shen, W. Jin, and R. Liu, "Density-based mixed platoon dispersion modelling with truncated mixed Gaussian distribution of speed," *Transportmetrica B, Transp. Dyn.*, vol. 3, no. 2, pp. 114–130, May 2015, doi: 10.1080/21680566.2014.960502.

[22] Y. Wei, C. Avcı, J. Liu, B. Belezamo, N. Aydın, P. Li, and X. Zhou, "Dynamic programming-based multi-vehicle longitudinal trajectory optimization with simplified car following models," *Transp. Res. B, Methodol.*, vol. 106, pp. 102–129, Dec. 2017.

[23] G. M. Pacey, "The progress of a bunch of vehicles released from a traffic signal," Road Res. Lab., Crowthorne, U.K., Res. Note RN/2665/GMP, 1956.

[24] B. Xu, X. J. Ban, Y. Bian, W. Li, J. Wang, S. E. Li, and K. Li, "Cooperative method of traffic signal optimization and speed control of connected vehicles at isolated intersections," *IEEE Trans. Intell. Transp. Syst.*, vol. 20, no. 4, pp. 1390–1403, Apr. 2019.

[25] C. Yu, Y. Feng, H. X. Liu, W. Ma, and X. Yang, "Integrated optimization of traffic signals and vehicle trajectories at isolated urban intersections," *Transp. Res. B, Methodol.*, vol. 112, pp. 89–112, Jun. 2018.

[26] M. Zhou, X. Qu, and S. Jin, "On the impact of cooperative autonomous vehicles in improving freeway merging: A modified intelligent driver model-based approach," *IEEE Trans. Intell. Transp. Syst.*, to be published.

[27] X. Luo, D. Wang, D. Ma, and S. Jin, "Grouped travel time estimation in signalized arterials using point-to-point detectors," *Transp. Res. B, Methodol.*, vol. 130, pp. 130–151, Dec. 2019.

[28] D. Ma, X. Luo, S. Jin, D. Wang, W. Guo, and F. Wang, "Lane-based saturation degree estimation for signalized intersections using travel time data," *IEEE Intell. Transp. Syst. Mag.*, vol. 9, no. 3, pp. 136–148, 2017.

HONGSHENG QI received the Ph.D. degree in transportation engineering from Jilin University. He is currently an Associate Professor of traffic engineering with Zhejiang University, Hangzhou, China. His research interests are in the areas of traffic control, traffic flow theory, and traffic information. He is especially interested in the traffic modeling, optimization and control under progressive connected and autonomous vehicles environment and network traffic analysis and diagnosis using big data. His webpage is https://person.zju.edu.cn/qihongsheng.

RUMENG DAI received the bachelor's degree in ocean engineering from Zhejiang University, in 2018. She is currently pursuing the master's degree with the Institute of Intelligent Transportation, Zhejiang University. Her research interests include traffic state analysis using big data and traffic congestion control.

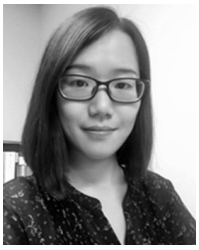

QING TANG received the bachelor's degree in information and computing science from the Hubei University of Education, and the master's degree in insurance in risk management from the Central University of Finance and Economics, China. She is currently pursuing the Ph.D. degree in transportation engineering with the Missouri University of Science and Technology. Her research focuses on big data analytics and applications, travel behavior, and transportation system modeling and simulation.

XIANBIAO HU received the Ph.D. degree from The University of Arizona, Tucson, AZ, USA, in 2013. He is currently an Assistant Professor with the Missouri University of Science and Technology (Missouri S&T, formerly University of Missouri, Rolla). His current research interests include the area of smart transportation systems, system modeling, and transportation data analytics.